Article

Rectangular Transition Metal-rTCNQ Organic Frameworks Enabling Polysulfide Anchoring and Fast Electrocatalytic Activity in Li-Sulfur Batteries: A Density Functional Theory Perspective

Jie-Zhen Xia [1,2,3,†], Lu-Chao Zhao [1,2,3,†], Man-Hua Liao [1,2,3,†] and Qi Wu [1,2,3,*]

1 School of Science, Tibet University, Lhasa 850000, China
2 Institute of Oxygen Supply, Center of Tibetan Studies (Everest Research Institute), Tibet University, Lhasa 850000, China
3 Key Laboratory of Cosmic Rays, Tibet University, Ministry of Education, Lhasa 850000, China
* Correspondence: wuqi@utibet.edu.cn
† The authors contributed equally to this work.

Abstract: Two-dimensional metal-organic frameworks (MOFs) have shown great development potential in the field of lithium-sulfur (Li-S) batteries. In this theoretical research work, we propose a novel $3d$ transition metals (TM)-embedded rectangular tetracyanoquinodimethane (TM-rTCNQ) as a potential high-performance sulfur host. The calculated results show that all TM-rTCNQ structures have excellent structural stability and metallic properties. Through exploring different adsorption patterns, we discovered that TM-rTCNQ (TM = V, Cr, Mn, Fe and Co) monolayers possess moderate adsorption strength for all polysulfide species, which is mainly due to the existence of the $TM-N_4$ active center in these frame systems. Especially for the non-synthesized V-rCTNQ, the theoretical calculation fully predicts that the material has the most suitable adsorption strength for polysul-fides, excellent charging-discharging reaction and Li-ion diffusion performance. Additionally, Mn-rTCNQ, which has been synthesized experimentally, is also suitable for further experimental con-firmation. These findings not only provide novel MOFs for promoting the commercialization of Li-S batteries, but also provide unique insights for fully understanding their catalytic reaction mecha-nism.

Keywords: metal-organic frameworks (MOFs); Li-S batteries; polysulfides; TM-rTCNQ

1. Introduction

With the ever-increasing development of society and the demand for energy storage systems, lithium-sulfur (Li-S) batteries (LiSBs) have been extensively investigated and considered as gifted candidates to replace Li-ion batteries [1], due to their extremely high energy density (~2600 W h kg^{-1}) and theoretical specific capacity (~1675 mA h g^{-1}) [2–7]. Another reason for the popularity of LiSBs is that sulfur hosts possess many advantageous attributes, such as low cost, high earth-abundance, non-toxicity and environmental benignity [6–9]. Despite these promising features, some persistent issues have been greatly re-stricting the commercial application of LiSBs. These problems mainly boil down to the following aspects [2,10–14]: (1) low electrical conductivity of elemental sulfur and the short-chain Li_2S/Li_2S_2 species, (2) the shuttle effect of the dissolved long-chain lithium pol-ysulfides (LiPSs), and (3) the sluggish charge-discharge reaction kinetics of whole electrochemical reaction process.

In this context, much attention has been focusing on exploiting novel cathode materials [15], which can facilitate the LiPSs conversion reactions and thus increase the sulfur utilization and cycle lifetime of LiSBs. For this purpose, a successful approach requires the utilization of polar materials including doped graphene [16], metal nanoparticles [17], metal-based compounds (e.g., borides [18,19], carbides [20], nitrides [7,21,22], oxides [23–25],

phosphides [26–29], sulfides [30–32]), defective borophene [33] and phosphorene [34], MXenes [2,35,36], metal organic frameworks (MOFs) [14,37–40], etc, as potential LiSBs host materials. Among these candidates, two dimensional (2D) MOFs displaying the charming features of large surface area [41,42] and tunable aperture sizes, have been highly concerned as one hopeful choice for sulfur hosts. However, research on the catalytic performance and mechanisms of these materials is still in its infant stage. Recently, various of 2D metal-7,7,8,8-tetracyanoquinodimethane (TCNQ) molecule coordination networks and TM-based 2D TCNQ monolayers have been synthesized [43–50]. Owing to the unique tetragonal (mainly rectangular and square) 2D lattice of atomic thickness, TCNQ has become an important building block for constructing novel func-tional nanomaterials with diverse properties (magnetic, optical, mechanical, electronic, etc). Furthermore, many theoretical studies have also shown that the TM-rCTNQ framework has great application potential in the NRR [51], ORR/OER [52], CO_2RR [53] and other electrocatalytic fields [54], but it has never been reported in the direction of LiSBs. On the basis of these exciting results, we speculate that TM-TCNQ can also be served as a potential anode material for improving the LiSBs performance.

Herein, we systematically explored the application of 2D TM-based rectangular TCNQ monolayers (referred to as TM-rTCNQ) in LiSBs based on first-principles calcula-tions. In addition to the structure that has been synthesized experimentally (Mn-rTCNQ [49], Ni-rTCNQ [47]), we also studied the performance of other $3d$ family TM-based rTCNQ (TM = Sc, Ti, V, Cr, Fe, Co and Cu) as highly efficient electrocatalysts for LiSBs. It was found that TM-rTCNQ (TM = V, Cr, Mn, Fe and Co) monolayers not only exhibit excellent metallic nature, but also have moderate binding strengths to polysulfides. Re-markably, the low energy barriers of the Li_2S decomposition are reduced to 0.88–1.41 eV, while the Li-ion diffusion barriers are in the range of 0.23–0.53 eV on TM-rTCNQ (TM = V, Cr, Mn, Fe and Co) monolayers, ensuring the rapid catalytic redox of LiPSs during the charge-discharge process. In a word, V-rTCNQ, as the most promising MOFs of all $3d$ family TM-rTCNQ structures, is very worthy to be prepared and have its performance verified, and the synthesized Mn-rTCNQ is also ready to be further confirmed experimen-tally. These findings offer a deep insight into the catalytic effects of novel 2D MOFs, as well as a promising strategy and general guidance for designing LiSBs.

2. Results and Discussion

2.1. Structure, Stability and Electronic Properties of TM-rTCNQ and S_8/LiPSs

The schematic diagram of the $2 \times 1 \times 1$ supercell of all $3d$ family TM-rTCNQ (TM = Sc, Ti, V, Cr, Mn, Fe, Co, Ni, Cu and Zn) structures is shown in Figure 1a, and black/red rectangular box areas represent the TM-rTCNQ unit cell and TCNQ molecule, respect-tively. Among them, each $3d$ TM atom is combined with four N atoms in TCNQ clusters. The detailed structural information is listed in Table S1. As observed in Figure S1, all at-oms lie in the same plane of TM-rTCNQ (TM = Sc, Ti, V, Cr, Mn, Fe, Co and Zn) mon-olayers. Some structural distortion of TM-N_4 center is observed for Ni-rTCNQ and Cu-rTCNQ, which is also consistent with related research works [51]. In addition, all the S_8/Li_2S_x (x = 1, 2, 4, 6, 8) species are fully optimized (Figure 1b) and are highly consistent with the previously reported theoretical calculations [16,55,56].

Additionally, the stability of these catalysts is evaluated by the energy difference (E_{diff}) between adsorption energies (E_a) and the average cohesive energies (E_{coh}). Gener-ally, systems with $E_{diff} = E_a - E_{coh} < 0$ represent that TM atoms can be atomically dis-persed on the TM-rTCNQ monolayers through the coordination effect. As shown in Fig-ure 1c, the E_a(TM) of TM-rTCNQ is within the range of $-4.19--9.95$ eV, which indicates the strong interaction between TM atoms and the N_4 active center. The negative values of E_{diff} reflect that all TM-rTCNQ configurations have sufficient structural stability to meet the possibility of experimental preparation. In addition, excellent electrical conductivity of the sulfur host materials is an important factor for practical Li-S battery applications. We focused on the conductivity of TM-rTCNQ and calculated the density of states (DOS) of all TM-rTCNQ

unit cells, as shown in Figure 1d and Figure S2. The TM-rTCNQ (TM = Sc, Ti, V, Cr, Mn, Fe, Co, Ni and Cu) structures, except for Zn-rTCNQ, all exhibit metallic prop-erties and are expected to improve the electrochemical performance of Li–S cells.
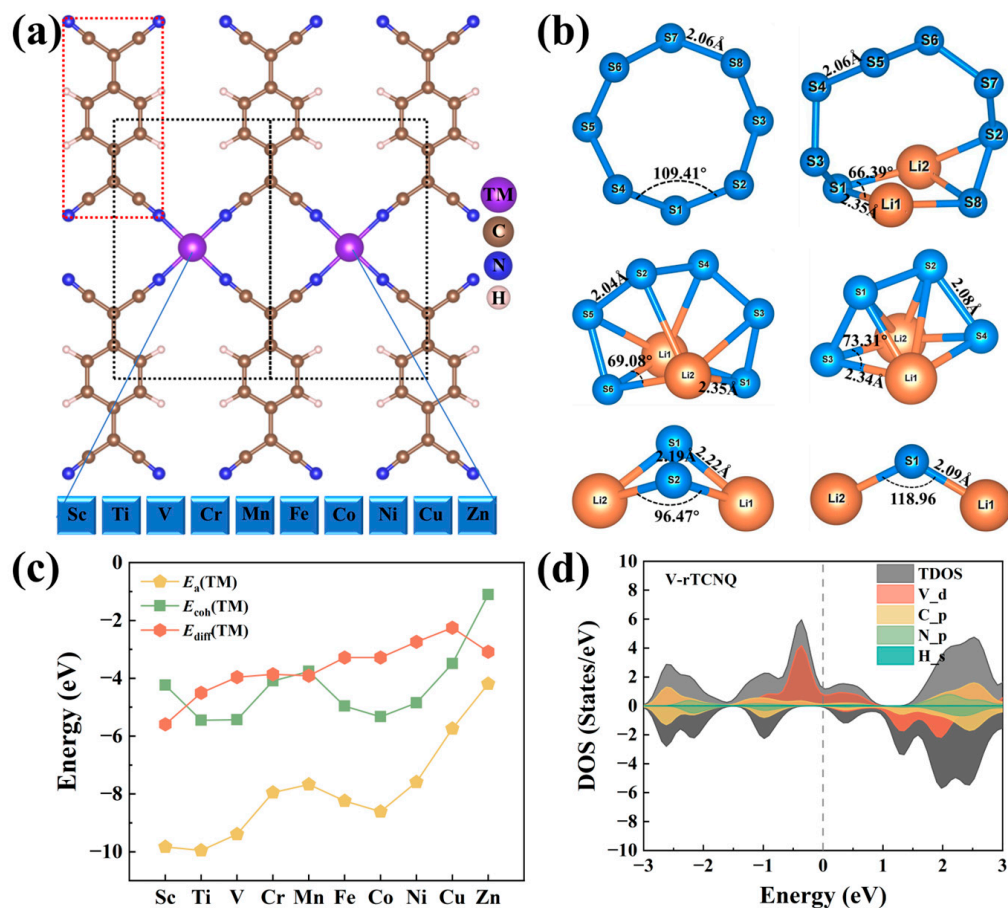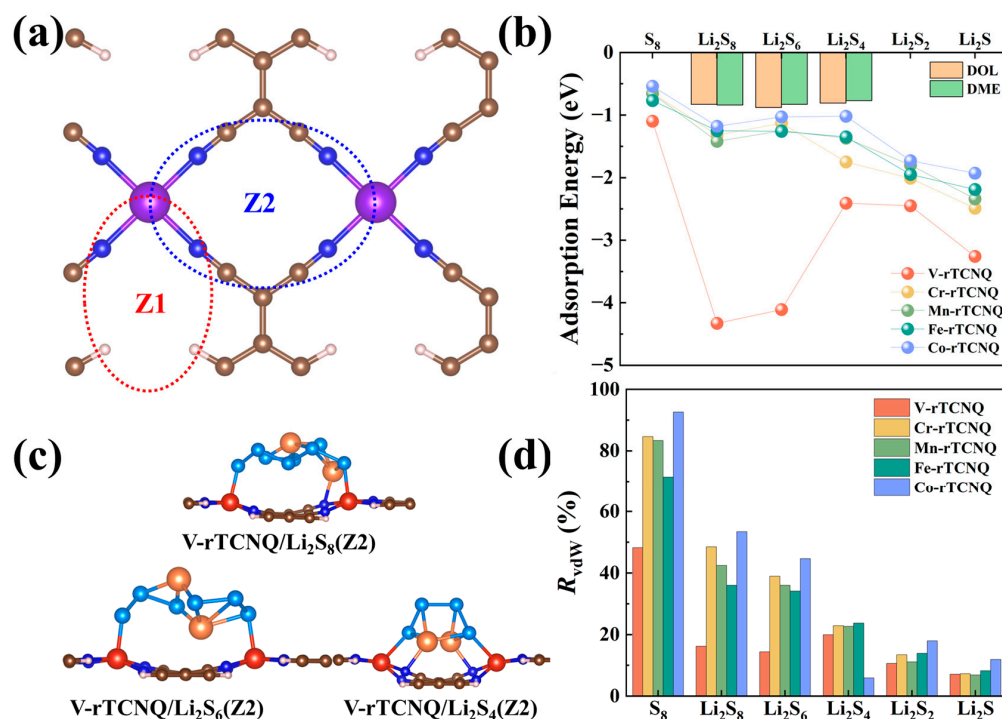

Figure 1. (**a**) Schematic diagram of TM-rTCNQ (TM = Sc, Ti, V, Cr, Mn, Fe, Co, Ni, Cu and Zn) geometric structures (the red and black rectangle boxes represent the TCNQ molecule and unit cell of TM-rTCNQ, respectively). (**b**) Fully optimized S_8/LiPSs molecules and some structural parame-ters are marked at corresponding positions. (**c**) The calculational results of adsorption energies (Ea), cohesive energies (E_{coh}) and E_{diff} ($E_a - E_{coh}$) of TM-rTCNQ. (**d**) The DOS diagram of V-rTCNQ unit cell, including total DOS (TDOS), projected DOS of *d* orbital of V (V_d), *p* orbital of C and N (C_p and N_p), as well as *s* orbital of H (H_s). Fermi-level is at the position of the gray dotted line.

2.2. Adsorption Performance of TM-rTCNQ for S_8/LiPSs

All well known, 1,3-dioxolane (DOL) and 1,2-dimethoxyethane (DME) electrolyte molecules can yield a competitive trapping to soluble Li_2S_4, Li_2S_6 and Li_2S_8. Therefore, the adsorption energies of Li_2S_4 (Li_2S_6, Li_2S_8) anchored on TM-rTCNQ substrates were first calculated. As displayed in the Figure S3, the energy range is from −0.88−−0.77 eV and mainly depends on Li-O bond interactions, which is highly in accordance with previous works [3]. An optimal host material should trap the soluble LiPSs more strongly than the DOL/DME solvent molecules to restrain the shuttle effect.

Herein, the adsorption energies of all TM-rTCNQ for polysulfides were calculated and shown in Figure 2b, Figures S4 and S5. We considered two adsorption patterns (Z1 and Z2). As shown in Figure 2a, Z1 mode involves trapping the LiPSs in the center of TM-N_4 coor-dination network, and Z2 mode refers to adsorbing the LiPSs with two TM atoms of the TM-rTCNQ supercell. It can be seen that Sc-rTCNQ and Ti-rTCNQ exhibit significant binding and structural distortion for S_8 and soluble LiPSs through Z2 mode

due to the strong interaction between two TMs and S atoms. Moreover, our results also show obvi-ous structural changes for the Ni-rTCNQ/Li$_2$S(Z1) and Cu-rTCNQ/Li$_2$S(Z1) adsorption systems. Therefore, TM-rTCNQ (TM = Sc, Ti, Ni and Cu) monolayers are ruled out since the structural integrity of the host is essential to the subsequent reactions. For the remain-ing TM-rTCNQ (TM = V, Cr, Mn, Fe and Co) structures, the adsorption energies of the most stable configurations for S$_8$/LiPSs on TM-rTCNQ are summarized in the Figure 2b. Obviously, these structures can effectively inhibit the shuttle effect problem and V- rTCNQ possesses the most outstanding adsorption performance shown in Figure 2c.


Figure 2. (**a**) Schematic diagram of Z1 and Z2 adsorption patterns. (**b**) The adsorption energies of TM-rTCNQ (V, Cr, Mn, Fe and Co) structures for S$_8$/LiPSs. (**c**) The top and side views of V-rTCNQ adsorbing Li$_2$S$_4$, Li$_2$S$_6$ and Li$_2$S$_8$ in Z2 pattern. (**d**) The ratio of van der Waals (R_{vdW}) interaction of TM-rTCNQ (V, Cr, Mn, Fe and Co) adsorbing S$_8$/LiPSs clusters.

Finally, the ratio of van der Waals (R_{vdW}) effect is shown in Figure 2d to further ana-lyze the physical or chemical interactions between TM-rTCNQ and polysulfides. According to Figure 2d, one can see that the effect of chemical binding is relatively increased along with the progression of the lithiation process. For example, the weight of vdW in-teraction contributing to the adsorption energy is 83.33% for the Mn-rTCNQ/S$_8$ system, whereas for Mn-rTCNQ/Li$_2$S, this ratio decreases to 6.84%. In addition, the vdW chemical interactions play a dominant role in the early transition metal decorated V-rTCNQ, with R_{vdW} in the range of 7.06–48.18%, leading to an impressive anchoring effect on S$_8$/LiPSs. Among them, the R_{vdW} of V-rTCNQ/Li$_2$S$_6$ and V-rTCNQ/Li$_2$S$_8$ adsorption systems is lower than that of V-rTCNQ/Li$_2$S$_4$, which is significantly related to the extremely strong adsorp-tion energy of V-rTCNQ for Li$_2$S$_6$ and Li$_2$S$_8$ clusters.

2.3. Electronic Structure Analysis

In order to further reveal the interactions of TM-rTCNQ configurations anchoring S$_8$/LiPSs, the charge density differences ($\Delta\rho$) and DOS were calculated. The $\Delta\rho$ and charge transfer amount of all adsorption systems of TM-rTCNQ (TM = V, Cr, Mn, Fe and Co) for S$_8$/LiPSs are displayed in the Figure 3a and Figure S6. One can see that the Li atoms of LiPSs form bonds with the N atoms on the V-rTCNQ surface, whereas the V atoms mainly

bond with the adjacent S atoms of S_8/LiPSs, as shown in Figure 3a. Moreover, Li_2S, Li_2S_2 and Li_2S_4 donate electrons to the V-rTCNQ host, whereas the high order Li_2S_6, Li_2S_8 and S_8 act as acceptors with the increase in S content.
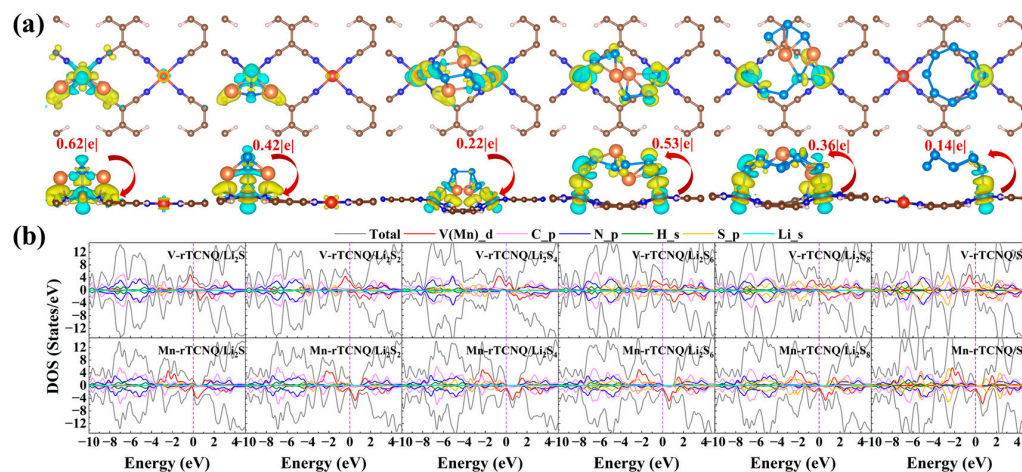
Figure 3. (**a**) The charge density differences and the charge transfer amount of the adsorption systems of V-rTCNQ for S_8/LiPSs. (**b**) The total and projected DOS of V-rTCNQ and Mn-rTCNQ after anchoring S_8/LiPSs clusters. Fermi-level in the violet dotted line is set to be zero.

Additionally, taking V-rTCNQ and Mn-rTCNQ as examples, the DOS of the adsorption systems were calculated and are plotted in Figure 3b. The metallic features of V-rTCNQ and Mn-rTCNQ are well maintained during the whole process, ensuring fast elec-tron transportation during the redox process of LiPSs. In addition, the tiny contribution of S_8 to the electronic states near the Fermi level is observed, manifesting the physical adsorption features. As Li ratio increases in the LiPSs, the *s* orbitals of lithium and *p* orbitals of N atoms have significant hybridization, verifying the formation of Li-N chem-ical bonds.

2.4. Charging-Discharging Catalytic and Li-ion Diffusion Capability

In addition to the anchoring effect for S_8/LiPSs, we also systematically investigated the catalytic performance of TM-rTCNQ for the whole charging-discharging process of LiSBs by simulation of the oxidation and reduction reactions of elemental sulfur, as well as the kinetic rate of Li-ion diffusion [2,12,57]. In this regard, the energy barriers of three dynamic processes were calculated based on DFT methods, and the summarized results are shown in Figure 4 and Figure S7, as well as in Tables S2 and S3. The Gibbs free energy ladder diagram of the sulfur reduction reactions (SRRs) process (discharging process) in Figure 4a shows that the reaction process from S_8 to *Li_2S_8 is basically exothermic, except for the V-rTCNQ conversion of *Li_2S_6 to *Li_2S_4, whereas the conversion process from *Li_2S_2 to *Li_2S is all endothermic. The rate-limiting step (RLS) of the whole catalytic reaction process is the *$Li_2S_2 \rightarrow$ *Li_2S, due to the maximum Gibbs free energy change ($\Delta G6$). As displayed in Figure 4a, $\Delta G6$ values for TM-rTCNQ (V, Cr, Mn, Fe and Co) are 3.15 eV, 3.28 eV, 3.36 eV, 3.50 eV and 3.68 eV respectively, and V-rTCNQ exhibits the smallest ΔG (3.15 eV) for RLS.

The first-step reaction of the charging process (Li2S dissociation: *$Li_2S \rightarrow$ *$LiS + Li^+ + e^-$) and the transition states of the Li-ion diffusion were also calculated using the CI-NEB method. The results show that V-rTCNQ and Co-rTCNQ have the lowest Li_2S decomposition and Li-ion diffusion barriers, respectively. The migration pathways of V-rTCNQ are plotted in the right side of Figure 4b, c (0 is the initial-state position and 4 is the final-state position), and those of other structures are shown in Figure S7. Figure 4b, c shows the minimum energy paths for Li diffusion on the surface of TM-rTCNQ (TM = V, Cr, Mn, Fe and Co). The reaction coordinates 1–3 stand for the intermediate images along the reaction path and reaction coordinate 3 is the transition state for the diffusion of Li-ions.

It is evi-dent that the dissociated single Li-ion moves far away from the center TM atoms to the N atoms of adjacent N_4 centers, accompanied by the fracture of the Li−S bonds. As shown in Table 1, our calculated results predict that un-synthesized V-rTCNQ and synthesized Mn-rTCNQ can be applied as sulfur hosts with excellent charging-discharging performance, and their RLS and Li_2S dissociation energy barriers are comparable with, or even lower than, those of SACs in the recent literature. The Li-ion diffusion behaviors of TM-rTCNQ (TM = V, Mn, Fe and Co) are also comparable with some other types of 2D material (the Li diffusion barrier is 0.66 eV for β_{12}-borophene [58], 0.38 eV for an InP_3 monolayer [59], 0.33 eV for graphene [60], 0.43 eV for C_3N [61], 0.35 eV for TiPc [12], etc.).
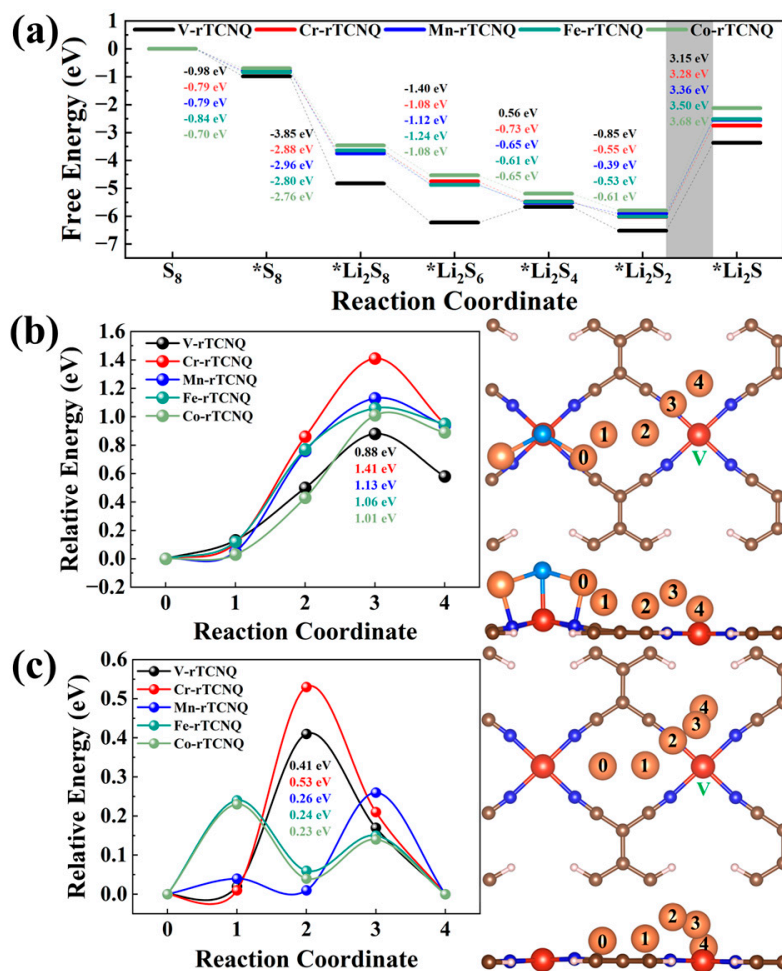
Figure 4. (**a**) The Gibbs free energy ladder diagram of SRRs process of V-rTCNQ, Cr-rTCNQ, Mn-rTCNQ, Fe-rTCNQ and Co-rTCNQ structures. (**b**,**c**) The relative energy profiles of TM-rTCNQ (TM = V, Cr, Mn, Fe and Co) and migration path of Li_2S decomposition or Li-ion diffusion on V-rTCNQ, respectively.

Table 1. The RLS and Li_2S dissociation barrier of V/Mn-rCTNQ and other SACs in some recent literatures.

Structures	RLS/eV	Energy Barrier (Li_2S Dissociation) /eV
V-rTCNQ	3.15	0.88
Mn-rTCNQ	3.36	1.13
VN_4@graphene [5]	4.24	0.70
TiPc [12]	4.33	0.86
VPc [12]	4.43	1.04
Ti-SnSe [62]	5.47	0.91

All in all, considering that V-rTCNQ has the most suitable adsorption strength for S_8/LiPSs clusters among all TM-rTCNQ, the lowest charging-discharging reaction energy barrier and acceptable Li-ion diffusion, it exhibits very promising value for LiSBs. Although the binding strength of Mn-rTCNQ to polysulfides is not the strongest, the en-ergy barrier of its discharging reaction is significantly lower than that of Fe-rTCNQ and Co-rTCNQ, and charging reaction performance is also batter than that of Cr-rTCNQ and is comparable with that of Fe-rTCNQ and Co-rTCNQ. What's more, the Li-ion diffusion energy barrier of Mn-rTCNQ is even lower than that of V-rTCNQ and Cr-rTCNQ, and it is very close to that of the best Co-rTCNQ. More importantly, this material has been pre-pared in experiments, thus also shows great application potential.

2.5. AIMD Simulation Results

In particular, long-term stability is a basic and vital element for application as a host material in LiSBs. Theoretically, AIMD simulations are further performed to ensure the thermal stability of TM-rTCNQ (TM = V, Cr, Mn, Fe and Co) substrates and adsorption systems. As representatives, TM-rTCNQ (TM = V, Cr, Mn, Fe and Co) monolayers and the adsorption systems of V-rTCNQ/Li_2S_4 (Li_2S_6, Li_2S_8) were chosen to implement AIMD sim-ulations with the NVT ensemble at 500 K for 10 ps. As displayed in Figure 5a and Figure S8, the geometries of the TM-rTCNQ (TM = V, Cr, Mn, Fe and Co) monolayers are well preserved when the temperature increases to 500 K. In addition, AIMD simulations were also carried out to check the overall thermal stability of the long-chain LiPSs (Li_2S_8, Li_2S_6 and Li_2S_4)- terminated V-rTCNQ systems. As detailed in Figure 5b–d, the results reveal that the sys-tems with adsorbed long-chain LiPSs and their hosts have no significant bond breakage and structural distortion. Our AIMD results show that the TM-rTCNQ monolayers and the adsorption systems of V-rTCNQ for soluble Li_2S_4 (Li_2S_6, Li_2S_8) pos-sess excellent ther-mal stability. Hence, V-rTCNQ can be further prepared and has great application poten-tial as a substrate that can greatly improve LiSBs performance. Last, but not least, synthe-sized Mn-rTCNQ is also extremely ready to be used in the experimental exploration of LiSBs.
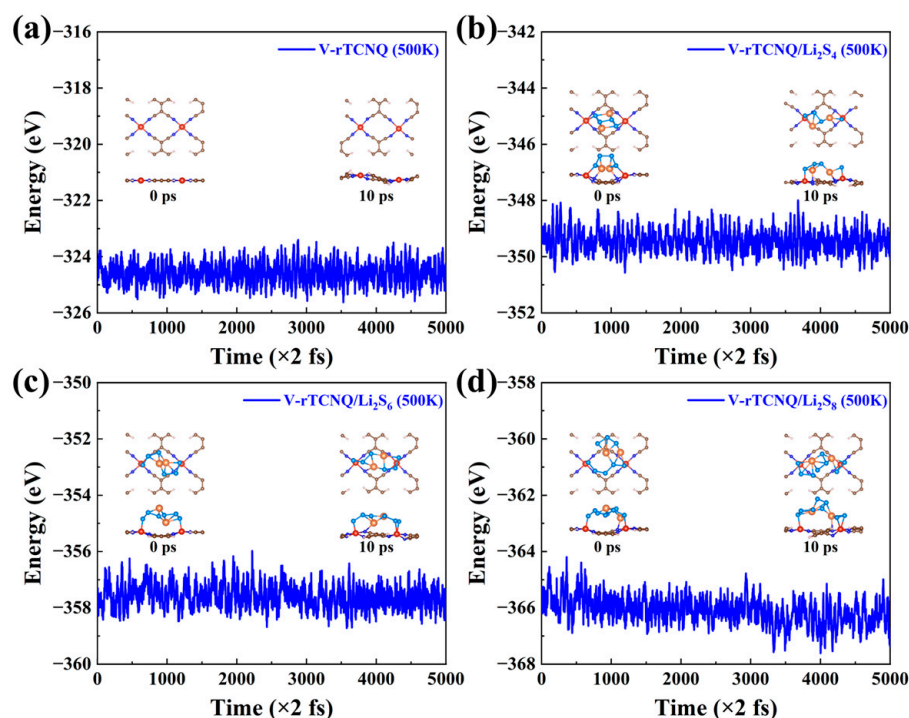
Figure 5. The AIMD simulation results of the V-rTCNQ structure (**a**) and adsorption systems of V-rTCNQ/Li_2S_4 (**b**), V-rTCNQ/Li_2S_6 (**c**), V-rTCNQ/Li_2S_8 (**d**) at 500 K and 10 ps.

3. Computational Details and Methods

3.1. Computational Details

In our work, all spin-polarized first-principles calculations were completed by the Vienna ab-initio Simulation Package (VASP) based on the density functional theory (DFT) [63]. The ion-electron interactions were described by the projector augmented wave (PAW) method [64] and the general gradient approximation (GGA) [65,66] in the Perdew–Burke–Ernzerhof (PBE) [67] form was used. The DFT-D3 [68] semi-empirical correction scheme of Gimme was adopted to treat the van der Waals (vdW) interaction between S_8/LiPSs and substrates. S_8 and Li_2S_x (x = 1, 2, 4, 6, 8) clusters were placed in a box of $20 \times 20 \times 20$ Å^3 to fully relax. A supercell, consisting of $2 \times 1 \times 1$ two-dimensional (2D) TM-rTCNQ monolayers, was utilized to anchor S_8/LiPSs, and the vacuum layer was set as 20 Å to eliminate the interactions between two periodic units. The simulation was run with a cutoff energy of 520 eV throughout the computations. These settings ensure convergence of the total energies and force within 10^{-5} eV and 0.02 eV/Å, respectively. The energy bar-riers of Li_2S decomposition and Li-ion diffusion were calculated using the climbing image nudged elastic band (CI-NEB) method [69,70]. Bader-charge analysis [71] was conducted to simulate the amount of charge transfer between TM-rTCNQ and S_8/LiPSs. Finally, ab-initio molecular dynamics (AIMD) simulations with a total time of 10 ps (5000 steps and step size set as 2 fs) were conducted to evaluate the thermal stability of TM-rTCNQ sub-strates and the adsorption systems of V-rTCNQ/Li_2S_4 (Li_2S_6 and Li_2S_8).

3.2. Computational Methods

Structural stability is one of the important factors for theoretically predicting the fea-sibility of experimental preparation of catalytic materials. It is understood that the TM-rTCNQ formed by the combination of TM and TNCQ can be fully judged through the adsorption energy (E_a), cohesion energy (E_c) and the difference (E_{diff}) between them [72,73]. Their detailed definitions are as follows:

$$E_a(\text{TM}) = E_{\text{TM}-\text{rTCNQ}} - E_{\text{support}} - E_{\sin\text{gle}-\text{TM}} \tag{1}$$

$$E_{\text{coh}}(\text{TM}) = \mu_{\text{TM}} - E_{\sin\text{gle}-\text{TM}} \tag{2}$$

$$E_{\text{diff}}(\text{TM}) = E_a(\text{TM}) - E_{\text{coh}}(\text{TM}) \tag{3}$$

where $E_{\text{TM}-\text{rTCNQ}}$, E_{support} and $E_{\text{single-TM}}$ are the total energies of TM-rTCNQ, the supports and isolated single transition metal (TM) atoms (TM = Sc, Ti, V, Cr, Mn, Fe, Co, Ni, Cu and Zn), respectively. μ_{TM} are the energies of TM in their stable bulk phase. When $E_{\text{diff}}(\text{TM}) < 0$, TM-rTCNQ can be considered as an experimental preparation and won't easily agglomerate into clusters.

In order to accurately evaluate the anchoring ability of TM-rTCNQ structures to S_8/LiPSs, the formula of adsorption energy (E_{ads}) is defined as [6,22]:

$$E_{\text{ads}} = E_{\text{TM}-\text{rTCNQ}+S_8/\text{LiPSs}} - E_{\text{TM}-\text{rTCNQ}} - E_{S_8/\text{LiPSs}} \tag{4}$$

where $E_{\text{TM}-\text{rTCNQ}+S_8/\text{LiPSs}}$, $E_{\text{TM}-\text{rTCNQ}}$ and $E_{S_8/\text{LiPSs}}$ are the total energies of the adsorption systems of TM-rTCNQ substrates with $E_{S_8/\text{LiPSs}}$ clusters, TM-rTCNQ monolayers and isolated S_8/LiPSs molecules, respectively. According to the above definition, more nega-tive E_{ads} corresponds to stronger adsorption interaction.

The charge density difference ($\Delta\rho$) is used to visualize the electron transfer between TM-rTCNQ and S_8/LiPSs, and its calculation formula is as follows [12,33]:

$$\Delta\rho = \rho_{\text{TM}-\text{rTCNQ}+S_8/\text{LiPSs}} - \rho_{\text{TM}-\text{rTCNQ}} - \rho_{S_8/\text{LiPSs}} \tag{5}$$

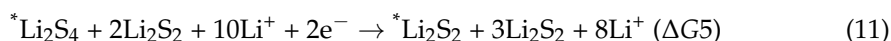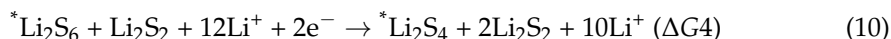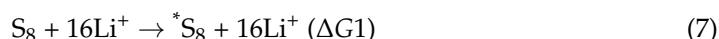where $\rho_{\text{TM}-\text{rTCNQ}+S_8/\text{LiPSs}}$, $\rho_{\text{TM}-\text{rTCNQ}}$ and $\rho_{S_8/\text{LiPSs}}$ are the charge density of adsorption systems, substrate materials and polysulfides, respectively.

To quantitatively analyze the degree of vdW and chemical interactions to determine the nature of the substrates' adsorption of polysulfides, the contribution ratio of vdW (R_{vdW}) interaction is calculated by the following formula [2,33]:

$$R_{vdW} = \frac{E_{ads}^{vdW} - E_{ads}^{without-vdW}}{E_{ads}^{vdW}} \times 100\% \tag{6}$$

where $E_{ads}^{with-vdW}$ and $E_{ads}^{without-vdW}$ stand for the adsorption energies with or without vdW correction.

The overall discharge reaction or sulfur reduction reactions (SRRs) process ($S_8 + 16Li^+ + 16e^- \rightarrow 8Li_2S$) of LiSBs can be depicted by following Equations (7)–(12) [5,6,12,62], where the S_8/LiPSs species with "*" indicate that they were adsorbed on the TM-rTCNQ. The energy of a single Li-ion and an electron ($Li^+ + e^-$) pair was treated as the energy of a crystalline Li atom.

$$S_8 + 16Li^+ \rightarrow {}^*S_8 + 16Li^+ \ (\Delta G1) \tag{7}$$

$${}^*S_8 + 16Li^+ + 2e^- \rightarrow {}^*Li_2S_8 + 14Li^+ \ (\Delta G2) \tag{8}$$

$${}^*Li_2S_8 + 14Li^+ + 2e^- \rightarrow {}^*Li_2S_6 + Li_2S_2 + 12Li^+ \ (\Delta G3) \tag{9}$$

$${}^*Li_2S_6 + Li_2S_2 + 12Li^+ + 2e^- \rightarrow {}^*Li_2S_4 + 2Li_2S_2 + 10Li^+ \ (\Delta G4) \tag{10}$$

$${}^*Li_2S_4 + 2Li_2S_2 + 10Li^+ + 2e^- \rightarrow {}^*Li_2S_2 + 3Li_2S_2 + 8Li^+ \ (\Delta G5) \tag{11}$$

$${}^*Li_2S_2 + 3Li_2S_2 + 8Li^+ + 8e^- \rightarrow {}^*Li_2S + 7Li_2S \ (\Delta G6) \tag{12}$$

The Gibbs free energy (ΔG) for above each elementary step was calculated as follows [5,12,14,62]:

$$\Delta G = \Delta E_{DFT} + \Delta E_{ZPE} - T\Delta S - neU \tag{13}$$

Herein, ΔE_{DFT} is directly obtained by electronic energy difference of each elementary reaction. ΔE_{ZPE} and $T\Delta S$ stand for zero-point energy and entropy change at 298.15 K, respectively. n and U are the number of electrons transferred and the applied voltage. For the battery systems, the ΔE_{ZPE} and $T\Delta S$ can be ignored in the calculation [11,12,62], therefore, when U = 0 V, $\Delta G \approx \Delta E_{DFT}$.

4. Conclusions

In our work, we systematically evaluated the potential application of all 3*d* family TM-rTCNQ (TM = Sc, Ti, V, Cr, Mn, Fe, Co, Ni, Cu and Zn) configurations in LiSBs. Among them, TM-rTCNQ (TM = V, Cr, Mn, Fe and Co) structures not only have excellent conductivity and structural stability, but also can produce appropriate adsorption strength for S_8/LiPSs to inhibit shuttle effects. V-rTCNQ is predicted to have excellent charging-discharging catalytic performance because of its lower RLS barrier (3.15 eV) and Li_2S dissociation barrier (0.88 eV) than many other 2D materials, as well as having a con-siderably low Li-ion diffusion barrier (0.41eV). AIMD simulation results reveal that the TM-rTCNQ (TM = V, Cr, Mn, Fe and Co) substrates and the adsorption system for soluble LiPSs onto V-rTCNQ are highly evaluated for their good thermodynamic stability at high temperatures. Additionally, the synthesized Mn-rTCNQ is also very worthy of further experimental confirmation and exploration. However, we also realize that obtaining ex-cellent substrate materials from a variety of constructed SACs is a relatively complicated process, which also indicates that future theoretical work needs to explore more rapid methods for comprehensively predicting the performance of LiSBs, such as high-through-put screening or machine learning. Nevertheless, our theoretical research still proposes a new candidate for exploring novel MOF catalysts with outstanding LiSBs catalytic perfor-mance and has great guiding significance for further experimental work.

References

1. Chen, S.; Jeong, S.R.; Tao, S. Key materials and future perspective for aqueous rechargeable lithium-ion batteries. *Mater. Rep. Energy* **2022**, *2*, 100096. [CrossRef]

2. Fan, K.; Ying, Y.; Luo, X.; Huang, H. Nitride Mxenes as sulfur hosts for thermodynamic and kinetic suppression of polysulfide shuttling: A computational study. *J. Mater. Chem. A* **2021**, *9*, 25391–25398. [CrossRef]

3. Singh, D.; Ahuja, R. Polypeptoid material as an anchoring material for Li–S batteries. *ACS Appl. Energy Mater.* **2021**, *4*, 13070–13076. [CrossRef]

4. Song, L.H.; Zhang, M.G.; Guo, J. First-principles study: Polyethylene glycol as a promising coating material for Li-S batteries. *Chem. Phys. Lett.* **2021**, *777*, 138711. [CrossRef]

5. Zeng, Z.; Nong, W.; Li, Y.; Wang, C. Universal-descriptors-guided design of single atom catalysts toward oxidation of Li_2S in lithium–sulfur batteries. *Adv. Sci.* **2021**, *8*, 2102809. [CrossRef]

6. He, C.; Liang, Y.; Zhang, W. Design of novel transition-metal-doped C_6N_2 with high-efficiency polysulfide anchoring and catalytic performances toward application in lithium-sulfur batteries. *ACS Appl. Mater. Interfaces* **2022**, *14*, 29120–29130. [CrossRef]

7. Ma, F.; Yu, B.; Zhang, X.; Zhang, Z.; Srinivas, K.; Wang, X.; Liu, D.; Wang, B.; Zhang, W.; Wu, Q.; et al. $WN_{0.67}$-embedded N-doped graphene-nanosheet interlayer as efficient polysulfide catalyst and absorbant for high-performance lithium-sulfur batteries. *Chem. Eng. J.* **2022**, *431*, 133439. [CrossRef]

8. Han, X.; Zhang, Z.; Xu, X. Single atom catalysts supported on N-doped graphene toward fast kinetics in Li–S batteries: A theoretical study. *J. Mater. Chem. A* **2021**, *9*, 12225–12235. [CrossRef]

9. Hua, W.; Li, H.; Pei, C.; Xia, J.; Sun, Y.; Zhang, C.; Lv, W.; Tao, Y.; Jiao, Y.; Zhang, B.; et al. Selective catalysis remedies polysulfide shuttling in lithium-sulfur batteries. *Adv. Mater.* **2021**, *33*, e2101006. [CrossRef]

10. He, J.; Chen, Y.; Manthiram, A. Metal sulfide-decorated carbon sponge as a highly efficient electrocatalyst and absorbant for polysulfide in high-loading Li_2S batteries. *Adv. Energy Mater.* **2019**, *9*, 1900584. [CrossRef]

11. Xia, J.; Cao, R.; Wu, Q. Transition metal decorated phthalocyanine as a potential host material for lithium polysulfides: A first-principles study. *RSC Adv.* **2022**, *12*, 13975–13984. [CrossRef]

12. Yu, B.; He, Q.; Zhao, Y. Exploring the anchoring effect and catalytic mechanism of 3*d* transition metal phthalocyanine for S_8/LiPSs: A density functional theory study. *Appl. Surf. Sci.* **2021**, *558*, 149928. [CrossRef]

13. Zhao, B.; Ren, Z.; Tan, G.; Li, Z.; Xie, J. Defects on Li_2S@graphene cathode improves the performance of lithium-sulfur battery, a theoretical study. *Acta Mater.* **2022**, *226*, 117632. [CrossRef]

14. Wang, J.; Li, F.; Liu, Z.; Dai, Z.; Gao, S.; Zhao, M. Two-dimensional conductive metal–organic frameworks as highly efficient electrocatalysts for lithium–sulfur batteries. *ACS Appl. Mater. Interfaces* **2021**, *13*, 61205–61214. [CrossRef]

15. Chang, Y.; Chen, J.; Zou, Z.; Li, J.; Wu, C.; Jiang, Y.; Chen, Y.; Zeng, Q.; Wu, X.; Sun, W.; et al. Labyrinth maze-like long travel-reduction of sulfur and polysulfides in micropores of a spherical honeycomb carbon to greatly confine shuttle effects in lithium-sulfur batteries. *Mater. Rep. Energy* **2022**, *2*, 100159. [CrossRef]

16. Yin, L.-C.; Liang, J.; Zhou, G.-M.; Li, F.; Saito, R.; Cheng, H.-M. Understanding the interactions between lithium polysulfides and N-doped graphene using density functional theory calculations. *Nano Energy* **2016**, *25*, 203–210. [CrossRef]

17. Gu, Q.; Qi, Y.; Chen, J.; Lu, M.; Zhang, B. Cobalt nanoparticles loaded on Mxene for Li-S batteries: Anchoring polysulfides and accelerating redox reactions. *Small* **2022**, *18*, e2204005. [CrossRef]

18. Xiao, Y.; Li, Y.; Guo, Z.; Tang, C.; Sa, B.; Miao, N.; Zhou, J.; Sun, Z. Functionalized Mo_2B_2 MBenes: Promising anchoring and electrocatalysis materials for lithium-sulfur battery. *Appl. Surf. Sci.* **2021**, *566*, 150634. [CrossRef]

19. He, J.; Bhargav, A.; Manthiram, A. Molybdenum boride as an efficient catalyst for polysulfide redox to enable high-energy-density lithium-sulfur batteries. *Adv. Mater.* **2020**, *32*, e2004741. [CrossRef]

20. Yu, B.; Huang, A.; Chen, D.; Srinivas, K.; Zhang, X.; Wang, X.; Wang, B.; Ma, F.; Liu, C.; Zhang, W.; et al. In situ construction of Mo_2C quantum dots-decorated cnt networks as a multifunctional electrocatalyst for advanced lithium-sulfur batteries. *Small* **2021**, *17*, e2100460. [CrossRef]

21. Ma, F.; Srinivas, K.; Zhang, X.; Zhang, Z.; Wu, Y.; Liu, D.; Zhang, W.; Wu, Q.; Chen, Y. Mo_2N quantum dots decorated N-doped graphene nanosheets as dual-functional interlayer for dendrite-free and shuttle-free lithium-sulfur batteries. *Adv. Funct. Mater.* **2022**, *32*, 2206113. [CrossRef]

22. Ma, F.; Zhang, X.; Sriniva, K.; Liu, D.; Zhang, Z.; Chen, X.; Zhang, W.; Wu, Q.; Chen, Y. NbN nanodot decorated N-doped graphene as a multifunctional interlayer for high-performance lithium–sulfur batteries. *J. Mater. Chem. A* **2022**, *10*, 8578–8590. [CrossRef]

23. He, Q.; Yu, B.; Wang, H.; Rana, M.; Liao, X.; Zhao, Y. Oxygen defects boost polysulfides immobilization and catalytic conversion: First-principles computational characterization and experimental design. *Nano Research* **2020**, *13*, 2299–2307. [CrossRef]

24. Liu, Y.T.; Liu, S.; Li, G.R.; Yan, T.Y.; Gao, X.P. High volumetric energy density sulfur cathode with heavy and catalytic metal oxide host for lithium-sulfur battery. *Adv. Sci.* **2020**, *7*, 1903693. [CrossRef] [PubMed]

25. Wang, L.; Song, Y.H.; Zhang, B.H.; Liu, Y.T.; Wang, Z.Y.; Li, G.R.; Liu, S.; Gao, X.P. Spherical metal oxides with high tap density as sulfur host to enhance cathode volumetric capacity for lithium-sulfur battery. *ACS Appl. Mater. Interfaces* **2020**, *12*, 5909–5919. [CrossRef]

26. Zhang, D.; Luo, Y.; Wu, B.; Zeng, P.; Xiang, C.; Zhao, C.; Sofer, Z.; Chen, M.; Wang, X. A heterogeneous FeP-CoP electrocatalyst for expediting sulfur redox in high-specific-energy lithium-sulfur batteries. *Electrochim. Acta* **2021**, *397*, 139275. [CrossRef]

27. Yuan, H.; Chen, X.; Zhou, G.; Zhang, W.; Luo, J.; Huang, H.; Gan, Y.; Liang, C.; Xia, Y.; Zhang, J.; et al. Efficient activation of Li_2S by transition metal phosphides nanoparticles for highly stable lithium–sulfur batteries. *ACS Energy Lett.* **2017**, *2*, 1711–1719. [CrossRef]

28. Zhang, C.; Du, R.; Biendicho, J.J.; Yi, M.; Xiao, K.; Yang, D.; Zhang, T.; Wang, X.; Arbiol, J.; Llorca, J.; et al. Tubular CoFeP@CN as a mott−schottky catalyst with multiple adsorption sites for robust lithium−sulfur batteries. *Adv. Energy Mater.* **2021**, *11*, 2100432. [CrossRef]

29. Ye, Z.Q.; Jiang, Y.; Qian, J.; Li, W.L.; Feng, T.; Li, L.; Wu, F.; Chen, R.J. Exceptional adsorption and catalysis effects of hollow polyhedra/carbon nanotube confined CoP nanoparticles superstructures for enhanced lithium-sulfur batteries. *Nano Energy* **2019**, *64*, 103965. [CrossRef]

30. He, J.; Hartmann, G.; Lee, M.; Hwang, G.S.; Chen, Y.; Manthiram, A. Freestanding 1T MoS_2/graphene heterostructures as a highly efficient electrocatalyst for lithium polysulfides in Li–S batteries. *Energy Environ. Sci.* **2019**, *12*, 344–350. [CrossRef]

31. He, J.; Bhargav, A.; Yaghoobnejad Asl, H.; Chen, Y.; Manthiram, A. 1T′-ReS_2 nanosheets in situ grown on carbon nanotubes as a highly efficient polysulfide electrocatalyst for stable Li–S batteries. *Adv. Energy Mater.* **2020**, *10*, 2001017. [CrossRef]

32. Seh, Z.W.; Yu, J.H.; Li, W.; Hsu, P.C.; Wang, H.; Sun, Y.; Yao, H.; Zhang, Q.; Cui, Y. Two-dimensional layered transition metal disulphides for effective encapsulation of high-capacity lithium sulphide cathodes. *Nat. Commun.* **2014**, *5*, 5017. [CrossRef]

33. Jiang, H.R.; Shyy, W.; Liu, M.; Ren, Y.X.; Zhao, T.S. Borophene and defective borophene as potential anchoring materials for lithium–sulfur batteries: A first-principles study. *J. Mater. Chem. A* **2018**, *6*, 2107–2114. [CrossRef]

34. Haseeb, H.H.; Li, Y.; Ayub, S.; Fang, Q.; Yu, L.; Xu, K.; Ma, F. Defective phosphorene as a promising anchoring material for lithium–sulfur batteries. *J. Phys. Chem. C* **2020**, *124*, 2739–2746. [CrossRef]

35. Zhao, Y.M.; Zhao, J.X. Functional group-dependent anchoring effect of titanium carbide-based MXenes for lithium-sulfur batteries: A computational study. *Appl. Surf. Sci.* **2017**, *412*, 591–598. [CrossRef]

36. Liu, S.; Song, Z.; Jin, X.; Mao, R.; Zhang, T.; Hu, F. Mxenes for metal-ion and metal-sulfur batteries: Synthesis, properties, and electrochemistry. *Mater. Rep. Energy* **2022**, *2*, 100077. [CrossRef]

37. Li, Y.; Lin, S.; Wang, D.; Gao, T.; Song, J.; Zhou, P.; Xu, Z.; Yang, Z.; Xiao, N.; Guo, S. Single atom array mimic on ultrathin mof nanosheets boosts the safety and life of lithium-sulfur batteries. *Adv. Mater.* **2020**, *32*, e1906722. [CrossRef]

38. Li, F.; Zhang, X.; Liu, X.; Zhao, M. Novel conductive metal-organic framework for a high-performance lithium-sulfur battery host: 2D Cu-benzenehexathial (BHT). *ACS Appl. Mater. Interfaces* **2018**, *10*, 15012–15020. [CrossRef]

39. Zheng, Y.; Zheng, S.; Xue, H.; Pang, H. Metal–organic frameworks for lithium–sulfur batteries. *J. Mater. Chem. A* **2019**, *7*, 3469–3491. [CrossRef]

40. Zhong, Y.; Xu, X.; Liu, Y.; Wang, W.; Shao, Z. Recent progress in metal–organic frameworks for lithium–sulfur batteries. *Polyhedron* **2018**, *155*, 464–484. [CrossRef]

41. Xu, B.; Masood Ul Hasan, I.; Peng, L.; Liu, J.; Xu, N.; Fan, M.; Niazi, N.K.; Qiao, J. Anion-regulation engineering toward Cu/In/MOF bimetallic electrocatalysts for selective electrochemical reduction of CO_2 to CO/formate. *Mater. Rep. Energy* **2022**, *2*, 100139. [CrossRef]

42. Zhong, Y.; Xu, X.; Wang, W.; Shao, Z. Recent advances in metal-organic framework derivatives as oxygen catalysts for Zinc-Air batteries. *Batter. Supercaps* **2018**, *2*, 272–289. [CrossRef]

43. Nafady, A.; O'Mullane, A.P.; Bond, A.M. Electrochemical and photochemical routes to semiconducting transition metal-tetracyanoquinodimethane coordination polymers. *Coord. Chem. Rev.* **2014**, *268*, 101–142. [CrossRef]

44. Vasylets, G.Y.; Starodub, V.A.; Barszcz, B.; Graja, A.; Medviediev, V.V.; Shishkin, O.V.; Bukrinev, A.S. Structure and spectral properties of TCNQ salts with Zn(II) and Ni(II) 2,2′-bipyridine complexes. *Synth. Met.* **2014**, *191*, 89–98. [CrossRef]

45. Abdurakhmanova, N.; Floris, A.; Tseng, T.C.; Comisso, A.; Stepanow, S.; De Vita, A.; Kern, K. Stereoselectivity and electrostatics in charge-transfer Mn- and Cs-$TCNQ_4$ networks on Ag(100). *Nat. Commun.* **2012**, *3*, 940. [CrossRef]

46. Shi, X.Q.; Lin, C.; Minot, C.; Tseng, T.-C.; Tait, S.L.; Lin, N.; Zhang, R.Q.; Kern, K.; Cerda, J.I.; Hove, M.A.V. Structural analysis and electronic properties of negatively charged TCNQ: 2D networks of $(TCNQ)_2Mn$ assembled on Cu(100). *J. Phys. Chem. C* **2010**, *114*, 17197–17204. [CrossRef]

47. Abdurakhmanova, N.; Tseng, T.C.; Langner, A.; Kley, C.S.; Sessi, V.; Stepanow, S.; Kern, K. Superexchange-mediated ferromagnetic coupling in two-dimensional Ni-TCNQ networks on metal surfaces. *Phys. Rev. Lett.* **2013**, *110*, 027202. [CrossRef]

48. Zhang, X.; Saber, M.R.; Prosvirin, A.P.; Reibenspies, J.H.; Sun, L.; Ballesteros-Rivas, M.; Zhao, H.; Dunbar, K.R. Magnetic ordering in TCNQ-based metal–organic frameworks with host–guest interactions. *Inorg. Chem. Front.* **2015**, *2*, 904–911. [CrossRef]

49. Faraggi, M.N.; Jiang, N.; Gonzalez-Lakunza, N.; Langner, A.; Stepanow, S.; Kern, K.; Arnau, A. Bonding and charge transfer in metal–organic coordination networks on Au(111) with strong acceptor molecules. *J. Phys. Chem. C* **2012**, *116*, 24558–24565. [CrossRef]

50. Tseng, T.-C.; Abdurakhmanova, N.; Stepanow, S.; Kern, K. Hierarchical assembly and reticulation of two-dimensional Mn- and Ni–$TCNQ_x$ (x = 1, 2, 4) coordination structures on a metal surface. *J. Phys. Chem. C* **2011**, *115*, 10211–10217. [CrossRef]

51. Lv, S.Y.; Huang, C.X.; Li, G.; Yang, L.M. Electrocatalytic mechanism of N_2 reduction reaction by single-atom catalyst rectangular TM-TCNQ monolayers. *ACS Appl. Mater. Interfaces* **2021**, *13*, 29641–29653. [CrossRef]

52. Deng, Q.; Zhao, J.; Wu, T.; Chen, G.; Hansen, H.A.; Vegge, T. 2D transition metal–TCNQ sheets as bifunctional single-atom catalysts for oxygen reduction and evolution reaction (ORR/OER). *J. Catal.* **2019**, *370*, 378–384. [CrossRef]

53. Liu, J.-H.; Yang, L.-M.; Ganz, E. Electrochemical reduction of CO_2 by single atom catalyst TM–TCNQ monolayers. *J. Mater. Chem. A* **2019**, *7*, 3805–3814. [CrossRef]

54. Deng, Q.; Wu, T.; Chen, G.; Hansen, H.A.; Vegge, T. Combinatorial selection of a two-dimensional 3d-TM-tetracyanoquinodimethane (TM-TCNQ) monolayer as a high-activity nanocatalyst for CO oxidation. *Phys. Chem. Chem. Phys.* **2018**, *20*, 5173–5179. [CrossRef]

55. Zhang, H.; Wang, S.; Wang, Y.; Huang, B.; Dai, Y.; Wei, W. Borophosphene: A potential anchoring material for lithium-sulfur batteries. *Appl. Surf. Sci.* **2021**, *562*, 150157. [CrossRef]

56. Rao, D.; Wang, Y.; Zhang, L.; Yao, S.; Qian, X.; Xi, X.; Xiao, K.; Deng, K.; Shen, X.; Lu, R. Mechanism of polysulfide immobilization on defective graphene sheets with N-substitution. *Carbon* **2016**, *110*, 207–214. [CrossRef]

57. Xu, Y.; Ou, X.; Zhang, X. Theoretical study of two-dimensional α-Tellurene with pseudo-heterospecies as a promising elemental anchoring material for lithium–sulfur batteries. *J. Phys. Chem. C* **2021**, *125*, 4623–4631. [CrossRef]

58. Grixti, S.; Mukherjee, S.; Singh, C.V. Two-dimensional boron as an impressive lithium-sulphur battery cathode material. *Energy Stor. Mater.* **2018**, *13*, 80–87. [CrossRef]

59. Wu, W.X.; Zhang, Y.M.; Guo, Y.H.; Bai, J.X.; Zhang, C.H.; Chen, Z.F.; Liu, Y.X.; Xiao, B.B. Exploring anchoring performance of InP_3 monolayer for lithium-sulfur batteries: A first-principles study. *Appl. Surf. Sci.* **2020**, *526*, 146717. [CrossRef]

60. Uthaisar, C.; Barone, V. Edge effects on the characteristics of Li diffusion in graphene. *Nano. Lett.* **2010**, *10*, 2838–2842. [CrossRef]

61. Wang, D.; Bao, Y.; Wu, T.; Gan, S.; Han, D.; Niu, L. First-principles study of the role of strain and hydrogenation on C_3N. *Carbon* **2018**, *134*, 22–28. [CrossRef]

62. Xiao, W.; He, Q.; Zhao, Y. Virtual screening of two-dimensional selenides and transition metal doped snse for lithium-sulfur batteries: A first-principles study. *Appl. Surf. Sci.* **2021**, *570*, 151213. [CrossRef]

63. Hafner, J. *Ab-initio* simulations of materials using VASP: Density-functional theory and beyond. *J. Comput. Chem.* **2008**, *29*, 2044–2078. [CrossRef] [PubMed]

64. Blochl, P.E. Projector augmented-wave method. *Phys. Rev. B Condens Matter* **1994**, *50*, 17953–17979. [CrossRef]

65. Juan, Y.M.; Kaxiras, E.; Gordon, R.G. Use of the generalized gradient approximation in pseudopotential calculations of solids. *Phys. Rev. B* **1995**, *51*, 9521–9525. [CrossRef]

66. Perdew, J.P.; Burke, K.; Ernzerhof, M. Generalized gradient approximation made simple. *Phys. Rev. Lett.* **1996**, *77*, 3865–3868. [CrossRef]

67. Hammer, B.; Hansen, L.B.; Norskov, J.K. Improved adsorption energetics within density-functional theory using revised perdew-burke-ernzerhof functionals. *Phys. Rev. B* **1999**, *59*, 7413–7421. [CrossRef]

68. Grimme, S.; Antony, J.; Ehrlich, S.; Krieg, H. A consistent and accurate ab initio parametrization of density functional dispersion correction (DFT-D) for the 94 elements H-Pu. *J. Chem. Phys.* **2010**, *132*, 154104. [CrossRef]

69. Henkelman, G.; Uberuaga, B.P.; Jónsson, H. A climbing image nudged elastic band method for finding saddle points and minimum energy paths. *J. Chem. Phys.* **2000**, *113*, 9901–9904. [CrossRef]

70. Sheppard, D.; Xiao, P.; Chemelewski, W.; Johnson, D.D.; Henkelman, G. A generalized solid-state nudged elastic band method. *J. Chem. Phys.* **2012**, *136*, 074103. [CrossRef]

71. Tang, W.; Sanville, E.; Henkelman, G. A grid-based bader analysis algorithm without lattice bias. *J. Phys. Condens. Matter* **2009**, *21*, 084204. [CrossRef]

72. Xu, H.; Cheng, D.; Cao, D.; Zeng, X.C. A universal principle for a rational design of single-atom electrocatalysts. *Nat. Catal.* **2018**, *1*, 339–348. [CrossRef]

73. Nong, W.; Qin, S.; Huang, F.; Liang, H.; Yang, Z.; Qi, C.; Li, Y.; Wang, C. Designing C_3N-supported single atom catalysts for efficient nitrogen reduction based on descriptor of catalytic activity. *Carbon* **2021**, *182*, 297–306. [CrossRef]